Ballistic Transport and Electrostatics in Metallic Carbon Nanotubes

Alexei Svizhenko, M. P. Anantram, and T. R. Govindan

***Abstract*—We calculate the current and electrostatic potential drop in metallic carbon nanotube wires self-consistently by solving the Green's function and electrostatics equations in the ballistic case. About one-tenth of the applied voltage drops across the bulk of a nanowire, independent of the lengths considered here. The remaining nine-tenths of the bias drops near the contacts, thereby creating a nonlinear potential drop. The scaling of the electric field at the center of the nanotube with length (L) is faster than $1/L$ (roughly $1/L^{1.25-1.75}$). At room temperature, the low bias conductance of larger-diameter nanotubes is larger than $4e^2/h$ due to occupation of noncrossing subbands. The physics of conductance evolution with bias due to Zener tunneling in noncrossing subbands is discussed.**

***Index Terms*—Ballistic transport, carbon nanotubes, inter-connects, modeling, nanowires.**

I. Introduction

CARBON nanotubes have the potential to make good interconnects because current densities approaching 10^9 A/cm^2 [1] and compatibility with silicon technology [2], [3] have been demonstrated. In the use of multiwall nanotubes for such applications, contact with as many layers of the tube as possible [4] is desirable. Larger diameter nanotubes are preferable because even the semiconducting shells can carry current due to small bandgaps. For example, a semiconducting shell with a radius of 18.8 nm has a half-bandgap of only 62.5 meV ($kT = 26$ meV at room temperature). Experimentally measured conductance of metallic carbon nanotubes is close to the theoretical maximum of $4e^2/h$ at low biases [5]–[8]. Experiments on small-diameter carbon nanotubes show that the differential conductance decreases with applied bias for voltages larger than 100–200 meV [9]–[11]. Reference [9] found that the conductance decrease with an increase in bias was caused by reflection of incident electrons at crossing subbands due to scattering with zone boundary phonons. Measured values of the mean free path (mfp) [12] are in the range of 0.1–1 μm at low bias and around 10 nm at high bias for 1.8-nm-diameter nanotubes (corresponds to a $(24,0)$ nanotube). Simple estimates of scattering rates [12], [13] show inverse dependence with nanotube diameter, which suggests that phonon scattering is less important in larger-diameter nanotubes. The noncrossing subbands of small-diameter nanotubes do not carry current due to their large bandgap. In contrast, larger-diameter nanotubes experimentally show an increase in conductance with applied bias [5], [6], [14], [15]. Reference [16] suggested that as the diameter increases, electrons may tunnel into noncrossing subbands, thus causing an increase in differential conductance with applied bias. The main drawbacks of the calculation in [16] was that the results depended on the assumed form of a potential drop in metallic nanotubes (charge self-consistency and phonon scattering were neglected). Apart from measuring current–voltage characteristics, the potential drop can be measured by electrostatic force microscopy (EFM). Reference [17] found that the potential drop in a single wall nanotube was small compared to a multiwall nanotube.

In this study, we computationally model ballistic electron flow in metallic nanowires within a tight-binding approximation by including *charge self-consistency*, which is an important factor in determining the current. The potential distribution and current–voltage characteristics are studied as a function of both nanotube diameter and length. In a one-dimensional (1-D) wire, even perfectly ballistic, the screening is poor due to the lower electron density of states. Reference [18] found that semiconducting-nanotube-based p-n junctions have a very long range $(\sim 1/\ln(y))$ tail in the charge distribution and, consequently, a nonzero electric field very far from the junction. It is, however, an open question whether metallic nanotubes also have poor screening properties. Here, we use an electrostatics model similar to that in [18], but significantly improve on transport, using nonequilibrium Green's function formalism. The ballistic approximation works well at low bias and/or in large-diameter nanotubes. The detailed study of phonon scattering effects will be given elsewhere.

The nature of the metallic contacts is also important. From an experimental viewpoint, the contact between a metal and a nanotube can either be an end or side contact. The end contact corresponds to only the nanotube tip, making the contact to the metal lead. In experiments, the end contacts usually include strong chemical modification of the nanotube at the metal–nanotube interface. Also, [5] found that end contacts without sufficient chemical modification of the nanotoube–metal interface have a large contact resistance. In such a configuration, electrons are injected directly from the metal to the nanotube region between the contacts. Due to the uncertainty of the contact band structure, modeling end contacts even remotely correct is extremely difficult.

The side contacts correspond to coupling between metal and nanotube atoms over many unit cells of the nanotube, and can be thought of as a nanotube buried inside a metal. Most experimental configurations correspond to side contacts [5], [19]. An

Manuscript received August 15, 2004; revised February 16, 2005.

The authors are with the Center for Nanotechnology, National Aeronautics and Space Administration (NASA) Advanced Supercomputing Division, NASA Ames Research Center, Moffett Field, CA 94035-1000 USA (e-mail: svizhenk@nas.nasa.gov; anant@nas.nasa.gov; govindan@nas.nasa.gov).

Digital Object Identifier 10.1109/TNANO.2005.851409

1536-125X/$20.00 © 2005 IEEE

Authorized licensed use limited to: University of Washington Libraries. Downloaded on July 28,2024 at 17:55:24 UTC from IEEE Xplore. Restrictions apply.

important feature of the side contacts is that the coupling between atoms in the nanotube is much stronger than coupling between the nanotube and metal atoms, which means that the band structure of the contacts can be assumed to be similar to that of the nanotube between the contacts. In the side-contact geometry, electrons are predominantly injected from the metal into the nanotube buried in the metal and then transmitted to the nanotube region between the contacts. In fact, as proof of such a process, scaling of conductance with the contact area has been observed in the side-contacted geometry by [5], [19]. Modeling showed that the conductance in metallic zigzag nanotubes can be close to the theoretical maximum for conductance with sufficient overlap area in the contact [20]. Here, we assume "perfect" contacts to represent an ideal side-contacted nanotube. The details of the contact model will be given below.

II. Formalism

In this paper, we consider only zigzag carbon nanotubes. The analysis for armchair nanotubes is similar. The general form of the Hamiltonian for electrons in a carbon nanotube can be written as

$$H = \sum_{i,x} U_x^i c_{i,x}^\dagger c_{i,x} + \sum_{i,j,x,x'} t_{x,x'}^{i,j} c_{i,x}^\dagger c_{j,x'}. \tag{1}$$

The sum is taken over all rings i, j in the transport direction and all atoms located at x, x' in each ring. We make the following common approximations: only nearest neighbors are included; each atom in an sp^2-coordinated carbon nanotube has three nearest neighbors, located $a_{cc} = 1.42$ Å away, and the band structure consists of only π-orbital with the hopping parameter $t_o = V_{pp\pi} = -2.77$ eV and the on-site potential $U_o = \epsilon_p = 0$. Within these approximations, only the following parameters are nonzero:

$$\begin{aligned} U_x^i &= U_o \qquad \forall i \\ t_{x,x'}^{i,i-1} &= t_{x,x'}^{i-1,i} = t_o \delta_{x\pm a/2,x'} \qquad \forall i = 2k \\ t_{x,x'}^{i,i+1} &= t_{x,x'}^{i+1,i} = t_o \delta_{x,x'} \qquad \forall i = 2k \end{aligned} \tag{2}$$

where $a = a_{cc}\sqrt{3}$. In $(N, 0)$ zigzag nanotubes, the wave vector in the circumferential direction is quantized as $\tilde{q} = 2\pi q/Na, q = 1, 2, \ldots, N$, creating eigenmodes in the energy spectrum. By doing a Fourier expansion of $c_{i,x}^\dagger$ and $c_{i,x}$ in $\tilde{q}$-space and using (2), we obtain a decoupled electron Hamiltonian in the eigenmode space

$$H = \sum_q H^q \tag{3}$$

$$H^q = \sum_i \left(U_{\tilde{q}}^i c_{i,\tilde{q}}^\dagger c_{i,\tilde{q}} + t_{\tilde{q}}^{i,i\pm1} c_{i,\tilde{q}}^\dagger c_{i\pm1,\tilde{q}} \right) \tag{4}$$

where

$$\begin{aligned} U_{\tilde{q}}^i &= U_o \qquad \forall i \\ t_{\tilde{q}}^{i,i-1} &= t_{\tilde{q}}^{i-1,i} = 2t_o \cos\left(\frac{\tilde{q}a}{2}\right) \equiv t_1 \qquad \forall i = 2k \\ t_{\tilde{q}}^{i,i+1} &= t_{\tilde{q}}^{i+1,i} = t_o \equiv t_2 \qquad \forall i = 2k. \end{aligned} \tag{5}$$

The 1-D tight-binding Hamiltonian H^q describes a chain with two sites per unit cell with on-site potential U_o and hopping parameters t_1 and t_2 (Fig. 1). For numerical solution, the spatial grid corresponds to the rings of the nanotube, separated by $a/2$ with a unit cell length of $3a/2 = 2.13$ Å, which is half the unit cell length of a zigzag nanotube. The subband dispersion relations are given by

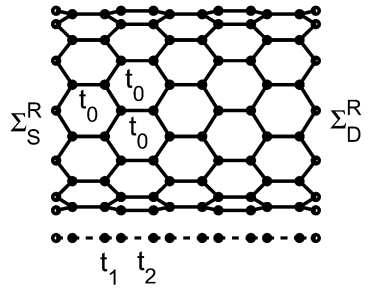


Fig. 1. Zigzag carbon nanotube and the corresponding 1-D chain. The hopping parameter between nearest neighbors in the nanotube is t_o. The 1-D chain has two sites per unit cell with on-site potential U_o and hopping parameters $t_1 = 2t_o \cos(\tilde{q}a/2)$ and $t_2 = t_o$.

$$E_q(k) = \pm\left|1 + 4\cos\left(\frac{3ak}{2}\right)\cos\left(\frac{q\pi}{N}\right) + 4\cos^2\left(\frac{q\pi}{N}\right)\right|^{1/2}. \tag{6}$$

Therefore, when $N = 3k$, there are two subbands with zero bandgap, and the tube is metallic. In the remainder of this paper, we distinguish between metallic or *crossing* subbands ($q = N/3$ and $2N/3$) and semiconducting or *noncrossing* subbands. The contacts are assumed to be reflectionless reservoirs maintained at equilibrium, i.e., they have well-defined chemical potentials, equal to that of the metal leads: V_S in the source and V_D in the drain. Further, the nanotube and metal are assumed to have the same work function. The contact self-energies $\Sigma_{c,q}^{R,<,>} = \Sigma_{S,q}^{R,<,>} + \Sigma_{D,q}^{R,<,>}$ due to the source contact are found [24] using the surface Green's function g_q^S of a semi-infinite nanotube, which is the solution of the following system of equations:

$$\begin{aligned} \left(a_1 - t_2^2 g_{2,q}^S\right) g_{1,q}^S &= 1 \\ \left(a_2 - t_1^2 g_{1,q}^S\right) g_{2,q}^S &= 1 \end{aligned} \tag{7}$$

where indexes 1 and 2 denote the two sites of the unit cell and $a_{1,2} = E - U_o - V_S$. The Green's function for the drain are solved in a similar way by making the following substitutions: $t_{1,2}^S \to t_{2,1}^D$ and $g_{1,2,q}^S \to g_{1,2,q}^D$. For each subband q, we solve a system of transport equations [24]

$$\left(E - H^q - V - \Sigma_{c,q}^R(E)\right) G^{R,q} = I \tag{8}$$

$$\left(E - H^q - V - \Sigma_{c,q}^R(E)\right) G^{<,>,q} = \Sigma_{c,q}^{<,>}(E) G^{A,q}. \tag{9}$$

Electron charge and current density n_i and J_i at each node i are found from the following equations:

$$n_i = -2i \sum_q \int_{-3t_o - eV_D}^{-eV_S + 10kT} G_{i,i}^{<,q}(E) \frac{dE}{2\pi} \tag{10}$$

$$J_i = \frac{4e}{\hbar} \sum_q \int_{-eV_D - 10kT}^{-eV_S + 10kT} G_{i,i+1}^{<,q}(E) t_{i+1,i}^q \frac{dE}{2\pi} \tag{11}$$

where we used the fact that the band bottom at equilibrium is at $-3t_o$. To integrate the electron charge over energy, we employed a conventional approach developed in density functional

Authorized licensed use limited to: University of Washington Libraries. Downloaded on July 28,2024 at 17:55:24 UTC from IEEE Xplore. Restrictions apply.

theory (DFT) [21]–[23] and described below. The technique drastically reduces the computational requirements as the whole band can be integrated with 200 energy grid points with an error of 10^{-6} of charge. The integral (10) is divided into equilibrium $[-3t_o - eV_D; -eV_D - 10kT]$ and nonequilibrium parts $[-eV_D - 10kT, -eV_S + 10kT]$. In the equilibrium part of the energy spectrum, the current is zero and $G^<(E) = -2if(E)\Im m[G^R(E)]$ where Fermi factor $f(E) = 1$ at these energies. G^R is analytical in the upper plain of complex energies, which allows one to transform the integration of $G^<$ over the real axis in the equilibrium part of the energy spectrum to the integration of G^R over a complex contour C starting at $-3t_o - eV_D$ and ending at $-eV_D - 10kT$. The nonequilibrium part is integrated over the real axis from $-eV_D - 10kT$ to $-eV_S + 10kT$

$$n_i = -\frac{2}{\pi}\sum_q \oint_C \Im m\left[G^{R,q}_{i,i}(E)\,dE\right] - \frac{i}{\pi}\sum_q \int_{-eV_D-10kT}^{-eV_S+10kT} G^{<,q}_{i,i}(E)\,dE. \quad (12)$$

In this study, corresponding to ballistic transport, we neglect electron–phonon scattering. The electron mfp is proportional to the matrix element squared and, thus, inversely proportional to the chirality index. Reference [12] reported $\lambda_o^{\rm el} \approx 1.6$ μm and $\lambda_o^{\rm in} \approx 10$ nm for a tube with a diameter of 1.8 nm, corresponding to a $(24, 0)$ nanotube. This allows us to assume that large-diameter nanotubes of moderate lengths, e.g., $\sim$100 nm $(240, 0)$ nanotube, will remain nearly ballistic even at high bias. The ballistic transport is also an adequate approximation at low bias for all diameter nanotubes due to the absence of strong inelastic phonon emission.

We model the electrostatics of the nanotube as a system of point charges between the two contacts located at $y = y_S = 0$ and $y = y_D = L$. The "perfect contacts" are modeled as parallel semi-infinite three-dimensional (3-D) metal leads that are maintained at fixed source and drain potentials: V_S for $y < y_S$ and V_D for $y > y_D$. Thus, while the self-energies due to contacts are identical to that of a semi-infinite nanotube, the role of electrostatics is included by image charges corresponding to a perfect metal. The electrostatic potential consists of a linear drop due to a uniform electric field created by the leads and the potential due to the charges on the tube and their images

$$V = -eV_S - e(V_D - V_S)(y - y_S)/(y_D - y_S) + \sum_j G(i,j)(n_j - N) \quad (13)$$

with the Green's function

$$G(i,j) = \frac{e}{4N\pi\epsilon_o}\sum_{n=-\infty}^{+\infty}\sum_l \left[\frac{1}{\sqrt{(y_i - y_j + 2nL)^2 + \rho_{k,l}^2}} - \frac{1}{\sqrt{(y_i + y_j + 2nL)^2 + \rho_{k,l}^2}}\right]. \quad (14)$$

Here, $\rho_{k,l}$ is the radial projection of the vector between atom k at ring i and atom l at ring j. The summation is performed over all atoms l at ring j for an arbitrary value of k. Maintaining the nanotube atoms buried in the metal at a fixed potential is close to reality because of the screening properties of 3-D metals. Within a few atomic layers from the metal surface, the potential should have approached the bulk values. While the variation in potential in these few atomic layers of the 3-D metal is not captured in our model, our conclusions on the nanotube electrostatics should not be significantly affected. The calculations for one bias point involve iterations of (7)–(13) until convergence of the potential and charge distributions is achieved. The solution of (8) and (9) employs the recursive algorithm [24], which scales linearly with the number of nodes. The contour integral in (12) is taken using Gaussian quadratures.

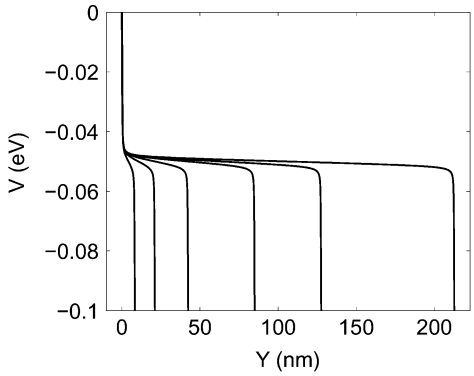


Fig. 2. Potential distribution versus position for $(12, 0)$ nanotubes of various lengths. The diameter of the $(12, 0)$ nanotube is 0.94 nm and the applied bias is 100 mV. Note the constant potential drop at the edges.

III. Results

A. Electrostatics

At low biases (100 mV), electron–phonon scattering does not play a significant role in determining the potential distribution for wires of moderate length (less than a few hundreds of a nanometer). The potential distribution for $(12, 0)$ nanotubes of lengths varying from 21.3 to 213 nm are shown in Fig. 2. The edges of the nanotube near the contact rapidly screen the applied bias/electric field. The screening is due to the free electron density provided by the crossing subbands. The potential drop is divided unequally between different parts of the nanotube with 90% of the applied bias dropping within 1 nm from the edges for both lengths considered here. Note, that in the ballistic regime, resistance of the nanotube does not depend significantly on tube length, which results in the drop at the edges being constant for all tube lengths. While the total density of states (DOS) per unit length of metallic nanotubes is independent of diameter, the DOS per subband and free charge carried by the crossing subbands are inversely proportional to the diameter. As a result, we find that the screening in metallic nanotubes degrades with diameter. The potential drop for nanotubes with diameters of 0.94 nm [$(12, 0)$ nanotube], 2.82 nm [$(36, 0)$] and 4.7 nm [$(60, 0)$] are shown in Fig. 3. Clearly, screening is poorer in the larger diameter nanotube. In fact, while the potential drops by 45 mV in a distance of 1 nm from the edge for the $(12, 0)$ nanotube, the potential drops for $(36, 0)$ and $(60, 0)$ are only 37 mV and 31 mV, respectively. The inset of Fig. 3 shows

Authorized licensed use limited to: University of Washington Libraries. Downloaded on July 28,2024 at 17:55:24 UTC from IEEE Xplore. Restrictions apply.

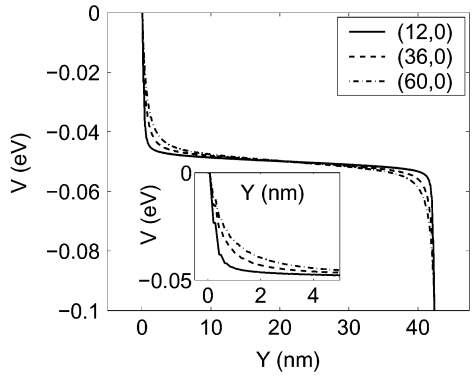


Fig. 3. Potential versus position for $(12,0)$, $(36,0)$, and $(60,0)$ nanotubes, with diameters 0.94, 2.82, and 4.7 nm. The screening for the larger-diameter nanotubes is poorer. The inset magnifies the potential close to the edge of the nanotube. The applied bias is 100 mV.

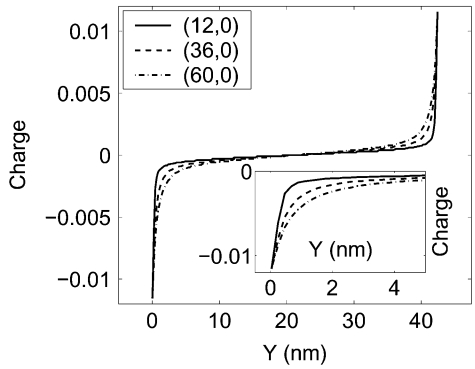


Fig. 4. Charge density versus position for $(12,0)$, $(36,0)$, and $(60,0)$ nanotubes. The inset magnifies the charge distribution close to the edge of the nanotube. The applied bias is 100 mV.

a substantially larger electric field away from the edges of the larger-diameter nanotube.

Fig. 4 shows the self-consistent charge profiles, corresponding to the potential in Fig. 3. The interplay between the competing factors of different DOS and electrostatic Green's function results in different charge profiles. In the larger diameter tubes more charge is accumulated at the edges. The electric field at the center of the nanotube as a function of length is shown in Fig. 5 for the tube with a diameter of 0.94 nm. We find that for all diameters, the electric field decreases more rapidly than $(1/L)$, where L is the length of the nanotube. The exact power law however depends on the diameter. If the computed electric field versus length is fit to $(1/L^a)$, the exponent a increases with increase in diameter. The value of a increases from 1.25 to 1.75 as the diameter increases from 0.94 to 18.85 nm. The dependence of the electric field on the chirality index of the tube is shown in Fig. 6. The electric field versus diameter $(D = aN/\pi)$ can be fit to D^b, where b is in the range of 0.25 and 0.75.

B. Transport

We now discuss the current–voltage characteristics as a function of bias for small- and larger-diameter nanotubes of length 42.6 nm, in the ballistic limit. The ballistic current and differential conductance for the different diameters are shown in Figs. 7 and 8. For the moderate diameter nanotubes $(N < 90)$,

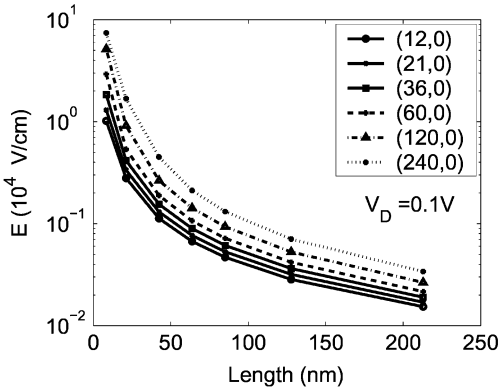


Fig. 5. This plot shows the electric field at the mid point versus nanotube length for various nanotube diameters at an applied bias of 100 mV. The electric field decreases approximately as $1/L^{1.25-1.75}$.

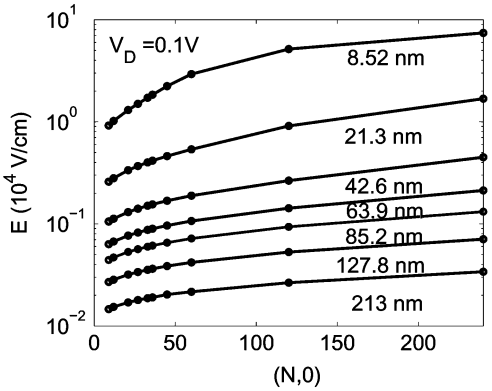


Fig. 6. Electric field at the midpoint versus nanotube chirality index for various lengths at an applied bias of 100 mV. The electric field increases approximately as $N^{0.25-0.75}$.

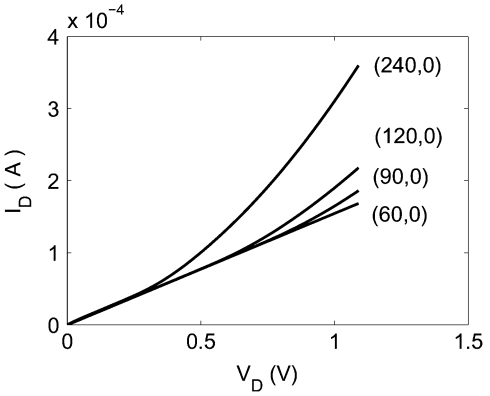


Fig. 7. Current–voltage characteristics of large-diameter nanotubes in the ballistic limit. The current shows a faster than linear increase with bias due to the contribution of noncrossing subbands.

only two crossing subbands contribute to transport. The current increases linearly with applied bias and the differential conductance is $4e^2/h$. In larger-diameter nanotubes ($N = 90, 120$, and 240), ballistic current shows super linear increase with bias. The conductance of larger-diameter nanotubes starts increasing after a threshold bias. This increase occurs due to Zener tunneling contribution of the noncrossing subbands: when the bias becomes larger than twice the bandgap of the lowest noncrossing subband, electrons can tunnel from valence band states $(E <$

Authorized licensed use limited to: University of Washington Libraries. Downloaded on July 28,2024 at 17:55:24 UTC from IEEE Xplore. Restrictions apply.

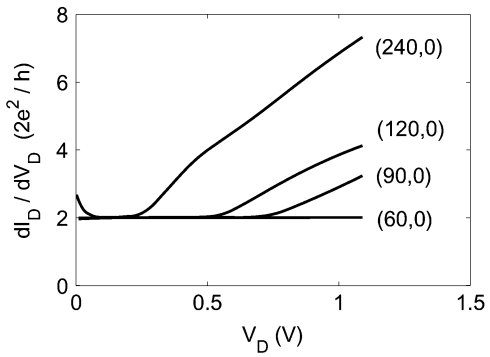


Fig. 8. Differential conductance as a function of bias in the ballistic case. Contribution of noncrossing subbands in the $(240,0)$ nanotube leads to the nonmonotonic behavior of conductance. High bias increase corresponds to Zener tunneling and is determined by the bandgap of the lowest noncrossing subband.

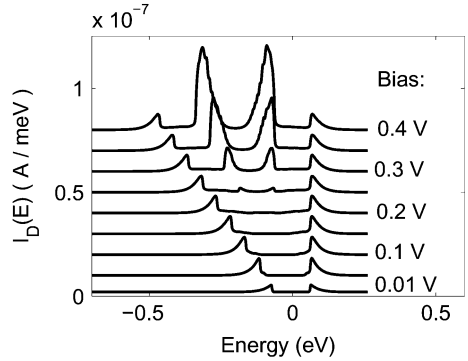


Fig. 10. Set of current density versus energy curves due to the lowest noncrossing subband in a $(240,0)$ nanotube under different biases. Two outermost peaks correspond to transport in the valence and conduction bands. Two inner peaks correspond to Zener tunneling between valence and conduction band states.

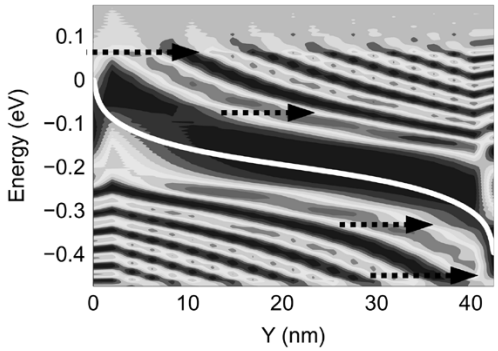


Fig. 9. Local density of states in the lowest noncrossing subband of a $(240,0)$ nanotube under a bias of 0.4 V as a function of position and energy. Brighter color shows higher DOS. Also shown is the potential profile. The arrows correspond to four contributions to a current due to the noncrossing subband in Fig. 10.

$-E_g^{\rm non}/2 + V(y)$) in the source to the conduction band states ($E > E_g^{\rm non}/2 + V(y)$) in the middle of the tube (the channel) and also from valence band states in the channel to the conduction band states in the drain. The lowest noncrossing subbands ($q = N/3 \pm 1$) in $(90,0), (120,0)$ and $(240,0)$ have bandgaps $E_g^{\rm non} = 331, 249$, and 125 meV, respectively, and start to contribute to current at biases of twice these values. In the ballistic limit, the self-consistently calculated current of $(240,0)$ nanotube at 1 V is 310 μA and the differential conductance is almost $13e^2/h$, signifying that a large number of subbands are contributing to current. As the barrier width at energies corresponding to valence band edge in the source E_v^S and conduction band edge in the drain E_c^D decreases with bias, the transmission and Zener tunneling current increase. The density of states (DOS) in the lowest noncrossing subband in $(240,0)$ nanotube at a bias of 0.4 V is shown in Fig. 9. Note the increased DOS in the bandgap at energies E_v^S and E_c^D. Another qualitative difference occurs at zero bias in the $(240,0)$ nanotube (Fig. 8). The zero bias conductance of $(240,0)$ nanotube is larger than $4e^2/h$ because the noncrossing subbands are partially filled and contribute to current: the first noncrossing subband opens at an energy of $2.4kT$ from the band center. This contribution is a simple intraband transport, determined by the population of the conduction band in the source and the valence band in the drain, but rather insensitive to the details of the potential distribution. At slightly higher biases, the noncrossing subband contribution to current saturates to a constant value and the contribution to differential conductance decreases to zero, while the total conductance decreases to $4e^2/h$.

To elucidate the effect of noncrossing subbands further, Fig. 10 shows the evolution with bias of current versus electron energy in the lowest noncrossing subband. At low biases, there are two peaks in the current density corresponding to partially filled valence and conduction bands. The height of the peaks increases only slightly and then saturates at all higher biases. These peaks in the current density are responsible for the increased value of zero-bias conductance. When bias is higher than twice the bandgap, two new peaks in the current density occur at E_v^S and E_c^D, corresponding to Zener tunneling at the source and drain, respectively. The height of these peaks increases rapidly due to the exponential dependence on the barrier width. The important consequence of the different origin of these four peaks is the temperature dependence of differential conductance. At low temperatures, the outermost peaks will vanish, reducing the value of conductance to $4e^2/h$. However, the height and shape of the inner peaks are insensitive to the temperature, which implies the robustness of Zener tunneling.

IV. Conclusion

We find that in the ballistic (low bias/large diameter) regime, applied bias drops mostly at the edges of metallic nanotubes. However, the 1-D nature of the nanotube leads to very slow ($\sim 1/L^{\alpha}$) screening of the electric field as compared to a bulk crystal. Our calculations show larger electric field for larger diameter nanotubes. The conductance of large-diameter nanotubes shows nonmonotonic bias dependence: at low and high bias, the conductance is higher than $4e^2/h$ due to the contribution of noncrossing subbands.

Acknowledgment

The authors would like to thank Dr. H. Mehrez, NASA Ames Research Center, Moffett Field, CA, for his help with the complex contour integration of DOS.

Authorized licensed use limited to: University of Washington Libraries. Downloaded on July 28,2024 at 17:55:24 UTC from IEEE Xplore. Restrictions apply.

REFERENCES

[1] B. Q. Wei, R. Vajtai, and P. M. Ajayan, "Reliability and current carrying capacity of carbon nanotubes," *Appl. Phys. Lett.*, vol. 79, pp. 1172–1174, Aug. 2001.

[2] F. Kreupl, A. P. Graham, G. S. Duesberg, W. Steinhogl, M. Liebau, E. Unger, and W. Honlein, "Carbon nanotubes in interconnect applications," *Microelectron. Eng.*, vol. 64, pp. 399–408, Oct. 2002.

[3] Q. Ngo, D. Petranovic, S. Krishnan, A. M. Cassell, Q. Ye, J. Li, M. Meyyappan, and C. Y. Yang, "Electron transport through metal–multiwall carbon nanotube interfaces," *IEEE Trans. Nanotechnol.*, vol. 3, no. 2, pp. 311–317, Jun. 2004.

[4] P. J. de Pablo, E. Graugnard, B. Walsh, R. P. Andres, S. Datta, and R. Reifenberger, "A simple, reliable technique for making electrical contact to multiwalled carbon nanotubes," *Appl. Phys. Lett.*, vol. 74, pp. 323–325, Jan. 1999.

[5] S. Frank, P. Poncharal, Z. L. Wang, and W. A. de Heer, "Carbon nanotube quantum resistors," *Science*, vol. 280, pp. 1744–1746, Jun. 1998.

[6] P. Poncharal, S. Frank, Z. L. Wang, and W. A. de Heer, "Conductance quantization in multiwalled carbon nanotubes," *Eur. Phys. J. D*, vol. 9, pp. 77–79, Dec. 1999.

[7] J. Nygard, D. H. Cobden, M. Bockrath, P. L. McEuen, and P. E. Lindelof, "Electrical transport measurements on single-walled carbon nanotubes," *Appl. Phys. A, Solid Surf.*, vol. 69, pp. 297–304, Sep. 1999.

[8] J. Kong, E. Yenilmez, T. W. Tombler, W. Kim, H. Dai, R. B. Laughlin, L. Liu, C. S. Jayanthi, and S. Y. Wu, "Quantum interference and ballistic transmission in nanotube electron waveguides," *Phys. Rev. Lett.*, vol. 87, pp. 106 801–106 804, Sep. 2001.

[9] Z. Yao, C. L. Kane, and C. Dekker, "High-field electrical transport in single-wall carbon nanotubes," *Phys. Rev. Lett.*, vol. 84, pp. 2941–2944, Mar. 2000.

[10] P. G. Collins, M. Hersam, M. Arnold, R. Martel, and P. Avouris, "Current saturation and electrical breakdown in multiwalled carbon nanotubes," *Phys. Rev. Lett.*, vol. 86, pp. 3128–3131, Apr. 2001.

[11] P. J. de Pablo, C. Gomez-Navarro, J. Colchero, P. A. Serena, J. Gomez-Herrero, and A. M. Baro, "Nonlinear resistance versus length in single-walled carbon nanotubes," *Phys. Rev. Lett.*, vol. 88, pp. 36 804–36 807, Jan. 2002.

[12] J. Park, S. Rosenblatt, Y. Yaish, V. Sazonova, H. Ustunel, S. Braig, T. A. Arias, P. W. Brouwer, and P. L. McEuen, "Electron–phonon scattering in metallic single-walled carbon nanotubes," *Nano Lett.*, vol. 4, pp. 517–520, Mar. 2004.

[13] G. Pennington and N. Goldsman, "Semiclassical transport and phonon scattering of electrons is semiconducting carbon nanotubes," *Phys. Rev. B, Condens. Matter*, vol. 68, pp. 045 426–045 436, Jul. 2003.

[14] P. Poncharal, C. Berger, Y. Yi, Z. L. Wang, and W. A. de Heer, "Room temperature ballistic conduction in carbon nanotubes," *J. Phys. Chem. B*, vol. 106, pp. 12104–12 118, Nov. 2002.

[15] Y. X. Liang, Q. H. Li, and T. H. Wang, "Current saturation in multiwalled carbon nanotubes by large bias," *Appl. Phys. Lett.*, vol. 84, pp. 3379–3381, Apr. 2004.

[16] M. P. Anantram, "Current-carrying capacity of carbon nanotubes," *Phys. Rev. B, Condens. Matter*, vol. 62, pp. R4837–R4840, Aug. 2000.

[17] A. Bachtold, M. S. Fuhrer, S. Plyasunov, M. Forero, E. H. Anderson, A. Zettl, and P. L. McEuen, "Scanned probe microscopy of electronic transport in carbon nanotubes," *Phys. Rev. Lett.*, vol. 84, pp. 6082–6085, Jun. 2000.

[18] F. Leonard and J. Tersoff, "Novel length scales in nanotube devices," *Phys. Rev. Lett.*, vol. 83, pp. 5174–5177, Dec. 1999.

[19] S. J. Tans, M. Devoret, H. Dai, A. Thess, R. E. Smalley, L. J. Geerligs, and C. Dekker, "Individual single-wall carbon nanotubes as quantum wires," *Nature*, vol. 386, pp. 474–477, Apr. 1997.

[20] M. P. Anantram, "Which nanowire couples better electrically to a metal contact: Armchair or zigzag nanotube?," *Appl. Phys. Lett.*, vol. 78, pp. 2055–2057, Apr. 2001.

[21] A. R. Williams, P. J. Feibelman, and N. D. Lang, "Green's-function methods for electronic-structure calculations," *Phys. Rev. B, Condens. Matter*, vol. 26, pp. 5433–5444, Nov. 1982.

[22] J. Taylor, H. Guo, and J. Wang, "*Ab initio* modeling of quantum transport properties of molecular electronic devices," *Phys. Rev. B, Condens. Matter*, vol. 63, pp. 245 407–245 419, Jun. 2001.

[23] M. Brandbyge, J.-L. Mozos, P. Ordejón, J. Taylor, and K. Stokbro, "Density-functional method for nonequilibrium electron transport," *Phys. Rev. B, Condens. Matter*, vol. 65, pp. 165 401–165 417, Mar. 2002.

[24] A. Svizhenko, M. P. Anantram, T. R. Govindan, and R. Venugopal, "Two-dimensional quantum mechanical modeling of nanotransistors," *J. Appl. Phys.*, vol. 91, pp. 2343–2354, Feb. 2002.



Alexei Svizhenko received the Ph.D. degree in electrical engineering from the University of Nebraska, Lincoln, in 1999, and the M.S. and B.S. degrees from the Moscow Institute of Physics and Technology, Moscow, Russia, in 1995 and 1993, respectively.

He is a Staff Scientist with the Center for Nanotechnology, National Aeronautics and Space Administration (NASA) Ames Research Center, Moffett Field, CA. His interests are in the modeling and computation of quantum transport in nanoscale transistors, carbon nanotubes, and novel devices.

Dr. Svizhenko was the recipient of the 2000 NASA Group Achievement Award and the 2003 and 2004 Computer Sciences Corporation Best Paper Award.



M. P. Anantram received the B.Sc. degree in applied sciences from the P.S.G. College of Technology, Coimbatore, India, in 1986, the M.Sc. degree in physics from the University of Poona, Pune, India, in 1989, and the Ph.D. degree from Purdue University, West Lafayette, IN, in 1995.

In 1997, he joined the National Aeronautics and Space Administration (NASA) Ames Research Center, Moffett Field, CA, following a post-doctoral fellowship with Purdue University and the University of California at Los Angeles (UCLA). He is currently Senior Scientist and Group Leader of computational nanoelectronics with the UARC, Center for Nanotechnology, NASA Ames Research Center. His main research focus is modeling and theory of semiconductor and molecular nanostructures such as nanotransistors, carbon nanotubes, and DNA.

Dr. Anantram was the recipient of the 1989 S. S. Joshi Award for academic excellence, the 2000 Veridian Technical Award for Best Paper for work on the electromechanical properties of carbon nanotubes, the NASA Group Achievement Award to the Nanotechnology Team, the 2002 CSC Best Paper Award for work on the electromechanical properties of carbon nanotubes, and the 2003 CSC Technical Excellence Award for work on modeling and theory of nanostructures.

T. R. Govindan received the Ph.D. degree in aerospace engineering from Pennsylvania State University, State College, in 1983.

He is currently a Senior Scientist with the National Aeronautics and Space Administration (NASA) Advanced Supercomputing Division, NASA Ames Research Center, Moffett Field, CA. His research interests include modeling low-temperature plasmas, transport in semiconductor devices and molecules, and the utilization of modeling in the emerging areas of nanotechnology, revolutionary computing, and sensing concepts. He is also additionally interested in fluid flow, multiphase reacting flow and phase transitions, and the development of numerical algorithms for modeling complex physical phenomena.

Authorized licensed use limited to: University of Washington Libraries. Downloaded on July 28,2024 at 17:55:24 UTC from IEEE Xplore. Restrictions apply.